*Egypt.J.Chem.* **Vol. 62**, No. 5. pp. 789 - 809 (2019)

**Egyptian Journal of Chemistry**
**http://ejchem.journals.ekb.eg/**

# $Fe_3O_4$ Nanoparticles: Synthesis, Characterization and Application in Removal of Iron from Aqueous Solution and Groundwater

**A.A. Swelam[1], M.B. Awad[1], Y.R. Gedamy[2] and A. Tawfik[1]**
[1]*Chemistry Department, Faculty of Science, Al-Azhar University, Cairo, Egypt.*
[2]*Hydrogeochemistry Dept., Desert Research Center, El-Matareya, Cairo, Egypt.*

MAGNETIC iron oxide nanoparticles were synthesized by co-precipitation method and characterized by using Fourier transform infrared spectroscopy (FT-IR), X-ray diffractometer (XRD), and scanning electron microscopy (SEM). Adsorption properties of the synthesized magnetic iron oxide nanoparticles towards iron ions were systematically investigated, including pH effect, adsorbent dosage, initial concentration, temperature, adsorption equilibrium and adsorption kinetics. The adsorption kinetics was studied by the pseudo first-order and pseudo second-order models. The adsorption isotherm for the removed iron ions were described by the Langmuir, Freundlich, D-R and Temkin isotherm models. The obtained results reveled that, the maximum adsorption capacity for Fe ions was 28.2mg/g and the removal percentage reached nearly 85% at adsorbent dosage 0.22g, temp. $60^0$C, time 210min., pH 4 and initial concentration 117.3mg/L. The adsorption capacity was increased with the increase of temperature and decrease of adsorbent dosage. The reaction obeyed both the pseudo second-order model and Langmuir isotherm model (with correlating constant $R^2$ is 0.98). Also, the calculated mean free energy of the sorption from the Dubinin–Radushkevich isotherm was found to be 207.7KJ/Mol for iron ions, indicating a chemical sorption. With high regression coefficients for Fe ions at 302K, and thermodynamic calculations suggested that the adsorption of iron ions onto the magnetic iron oxide nanoparticles is an endothermic process.

**Keywords:** Magnetic iron oxide nanoparticles, Heavy metals ions, Adsorption isotherms, Kinetics, Thermodynamics.

## Introduction

Water pollution that caused by toxic heavy metals is a worldwide environmental problem because of its adverse effects on human health, as well as on aquatic flora and fauna. Disposal of heavy metals directly or indirectly in the soils and water resources causes significant environmental risks, due to their high toxicity, non-biodegradability, and prevalent occurrence in nature [1,2].

Among the heavy metals, iron (Fe) has been identified as one of the significant toxic elements found in various industrial wastewaters. Iron is an essential trace element of great importance for humans, animals and plants. Iron is a vital element in most biological systems like photosynthetic and respiratory electron transport, nitrate reduction, chlorophyll synthesis and detoxification of reactive oxygen species in plants and plays a key role in the transport of oxygen in the body. Most iron-containing proteins contain ferric ions, at least transiently. Well studied examples include iron–sulphur clusters, oxyhemoglobin, ferritin, and the cytochromes. The oxidation ability of iron is a leading cause of poisoning in the human body [3].

Gulp of large amounts of iron salt causes vomiting and intestinal bleeding [4]. A high iron concentration within water pipelines promotes undesirable bacterial growth (iron bacteria), resulting in the deposition of a slimy coating

*Corresponding author e-mail: ahmed_bedair30@hotmail.com
Received 15/10/2018; Accepted 8/1/2019
DOI: 10.21608/EJCHEM.2019.5527.1488
©2019 National Information and Documentation Center (NIDOC)

on the pipelines [5]. For the previous reasons, removal of iron ions from water resources is urgent. Noteworthy, the removal techniques for metal ions have been developed in recent years.

Nanoparticles have high adsorption capacities and large specific surface areas. They are highly mobile in porous media because of their specific functionality, surface area per unit mass and smaller size than the relevant pore spaces and the ease of modifying their surface functionality [6, 7].

Recently, magnetic nanoparticles (MNP) such as $Fe_3O_4$ and $\gamma$-$Fe_2O_3$ have been utilized to remove toxic metal ions, radioactive elements, microbial pathogens and organic dyes from water and wastewater [8,9,10]. The magnetic iron oxide nano-materials are generally unstable in strong acidic solutions and undergo leaching that leads to reduction the lifetime of such materials.

Further limitation is based on the large ratio of surface area to volume that leads to aggregation of particles (magnetic and van der Waals) and thus a minimization in their surface energy [11,12,13]. Furthermore, magnetic nanoparticles functioned or coated with organic/inorganic molecules, surfactant, polymers and dendrimers are more effective for the free functional groups present on the surface due to providing a large number of active sites as well as aqueous stability, which is necessary for the successful adsorption of metal ions [14]. This approach prevents the agglomeration of magnetic nanoparticles as well as providing an environment for the transferring of hydrophobic iron oxide nanoparticles into a hydrophilic system.

El-Sadat City is one of the newly constructed industrial settlements in the western desert fringes surrounding the Nile Delta. El-Sadat City has received special attention during the last few decades due to its reasonably good groundwater resources. Groundwater is the only source of drinking water, as well as for domestic, industrial and agricultural purposes. Over-exploitation of the groundwater to meet all the potential needs could facilitate the migration of the accumulated pollutant to reach the underlying groundwater. Contamination of groundwater due to different activities could therefore severely endanger survival in this harsh environment. The occurrence of heavy metals in industrial and municipal sewage effluents is of interest because they are often present at significant levels and if infiltrated to groundwater can have severe effects on public health. An understanding of groundwater origin, sources, ages, migration pathway mixing rates and pollution sources is necessary for the viable long-term development of El-Sadat City.

Sadat city is the second new industrial city built in Egypt (Fig.1). It is located in the north-west of Cairo at the point 93km on Cairo-Alexandria desert road with a total area of 500km$^2$. It is located between 30$^o$ 30$^/$ and 30$^o$ 50$^/$ E, and 30$^o$ 18$^/$ and 30$^o$ 30$^/$ N. Sadat city was built as residential, industrial, and agriculture city. The study area includes oxidation ponds, a wooded area irrigated with treated wastewater from the oxidation pond,

**Fig. 1. Location map of the study area**

**TABLE 1. The heavy metals concentrations (ppm)in the selected water samples at the study area.**

| Water sample | Cr | Cu | Fe | Mn | Pb | Zn | Co |
|---|---|---|---|---|---|---|---|
| 1 | 0.0063 | 0.0601 | 1.136 | 0.2581 | 0.0172 | 0.1145 | 0.0062 |
| 2 | 0.0092 | 0.0081 | 0.4402 | 0.1502 | 0.0044 | 0.0581 | 0.0008 |
| 3 | 0.0074 | 0.0079 | 0.2975 | 0.0005 | 0.0004 | 0.0161 | 0.0017 |
| 4 | 0.0078 | 0.0283 | 2.800 | 0.7008 | 0.0049 | 0.8282 | 0.0011 |

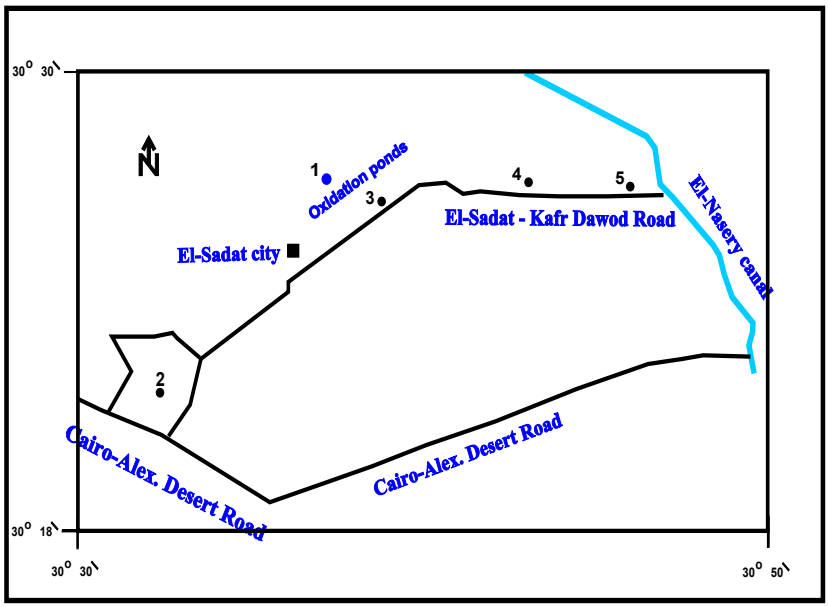


**Fig. 2. Water samples sites map.**

another area irrigated with groundwater and a non-cultivated area.

## Materials and Methods

*Sampling*

One surface water sample and four groundwater samples were selected and collected from the study area. Those collected water samples analyzed at the laboratory of Desert Research Center to detect the inorganic pollutants (soluble heavy metals) in them (Table 1 and Fig.2).

*Sorbent*

All of the chemicals and reagents ($FeCl_3 \cdot 6H_2O$, $FeSO_4 \cdot 7H_2O$, HCl and Ethanol) used were of analytical grade with the mass fraction purity of 0.99 and used as received without further purification where they supplied by Merck (India) and from British Drug House, Poole(England). Ferric chloride stock solutions were prepared by dissolving a desired amount of the metal salt in 0.5% HCl to prevent hydrolysis and the working solution was prepared daily with the required dilution. The pH was adjusted using 0.1 M HCl and NaOH.

*Preparation and characterization of magnetic iron oxide nanoparticles*

Ferromagnetic $Fe_3O_4$ nanoparticles were synthesized with an eco-friendly method modified by Peng et al, 2012[15]. The $Fe_3O_4$nanoparticles were synthesized in-situ by co-precipitation method, which is a classical method for $Fe_3O_4$ generation. Briefly, 6.1g of $FeCl_3 \cdot 6H_2O$ dissolved in 100ml of distilled water, followed by addition of a few drops of concentrated HCl in order to avoid $Fe(OH)_3$ precipitation, afterwards 4.2g of $FeSO_4 \cdot 7H_2O$ were also dissolved in a mixture and heated to 90°C, then 10ml of $NH_4OH$ (25%) was added rapidly, and pH of the solution was maintained at 10. The mixture was stirred at 90°C for 30min and then cooled to room temperature. The black substance was collected by centrifugation at 3,000rpm and washed to neutral with ethanol and distilled water [16]. The chemical reaction of $Fe_3O_4$ formation can be

written as in Eq.1:

$$Fe^{2+} + 2Fe^{3+} + 8OH^- \rightarrow Fe_3O_4 + 4H_2O\text{--------} \quad (1)$$

*Characterization*

*FT-IR spectroscopy*

Detailed structural and compositional studies were carried out using a FT-IR 200 TERMO spectrometer(Al-Azhar University laboratories, Cairo, EGYPT). Figure 3 presents the magnetic iron oxide nanoparticle FTIR spectra before (a) and after (b) loading with iron. The bands from 571.94 to 408.83cm$^{-1}$ are assigned to characteristic Fe–O vibrations of $Fe_3O_4$. The band at 1632.09cm$^{-1}$ is due to bending modes of the water molecules adsorbed on the iron oxide surfaces. Many O–H vibrations occur at 3406.25 and the peaks at 1406.53cm$^{-1}$ are characteristics of the bending of the O-H group. Slight differences occur at the peaks at 571.94 to 408.83cm$^{-1}$ representing Fe–O and –OH functions, respectively, before and after iron adsorption was observed. The peak at 571.94 shifted to 571.78cm$^{-1}$corresponding to formation of Fe–O–Fe on the active sites of the iron oxide surfaces. The typical inverse spinel ferrite structure involves two IR absorption bands, one at around

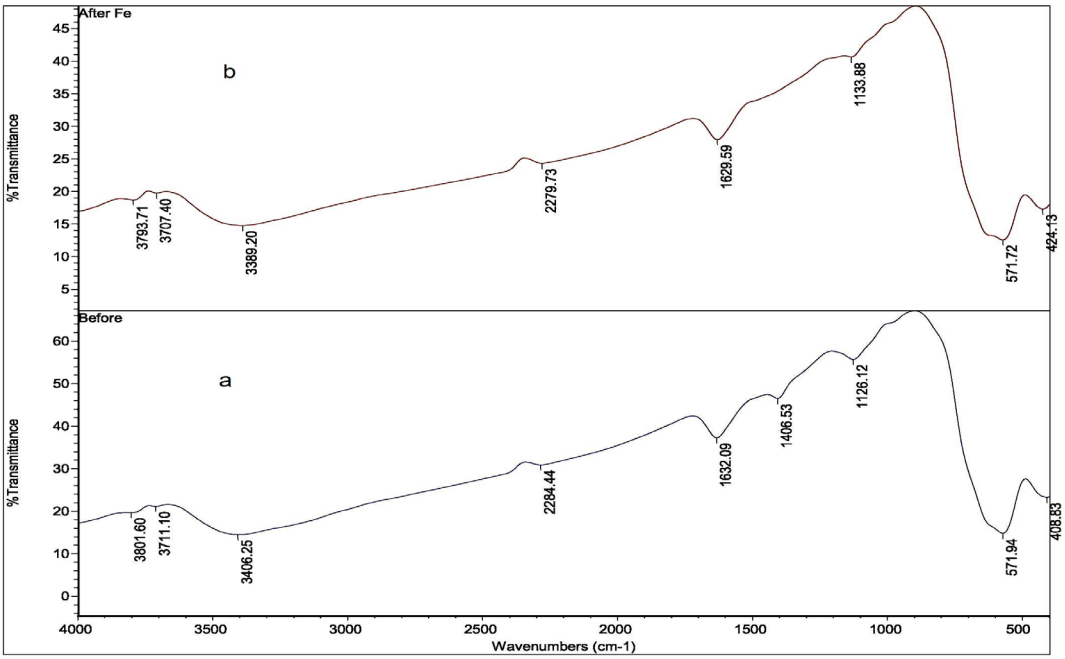


**Fig. 3. FTIR spectra of the iron oxide before (a) and after (b) Fe ions loaded on magnetic iron oxide nanoparticles.**

400cm$^{-1}$ which attributes to stretching vibration of tetrahedral groups $Fe_3 + O_2$ – [17]. Some peaks can be seen to have disappeared from the iron oxide. The peaks initially at 1406.53 and 1126.12cm$^{-1}$ disappeared after iron adsorbed on iron oxide, indicating their participation in Fe adsorption. Furthermore, a significant shift in peaks (1632–1630cm$^{-1}$) suggested that an interaction occurred between the active sites of the adsorbent and the removed Fe ions. Moreover, a distinctive reduction in intensities of some peaks indicated their involvement in the adsorption process [18].

*X-ray powder diffraction*

X-ray diffraction (XRD) patterns for magnetic and nonmagnetic energy cane biochars were obtained on a powder X-ray diffraction (XRD) system under X-ray microanalyzer (Module Oxford 6587 INCA x-sight) attached to JEOL JSM-5500 LV scanning electron microscopy at 20KV after gold coating using SPI-Module sputter coater at the Regional Center of Mycology and Biotechnology, Cairo, Egypt.

The X-ray diffraction (XRD) analysis was carried out to investigate the composition and crystal structure of the prepared samples. Figure 4 (a and b) showed the XRD patterns of the pure and composite adsorbent. There are seven characteristic diffraction peaks of the prepared magnetite iron oxide nanoparticles. The diffraction peaks at 18.3°, 30.1°, 35.5°, 43.1°, 53.48°, 57.05°

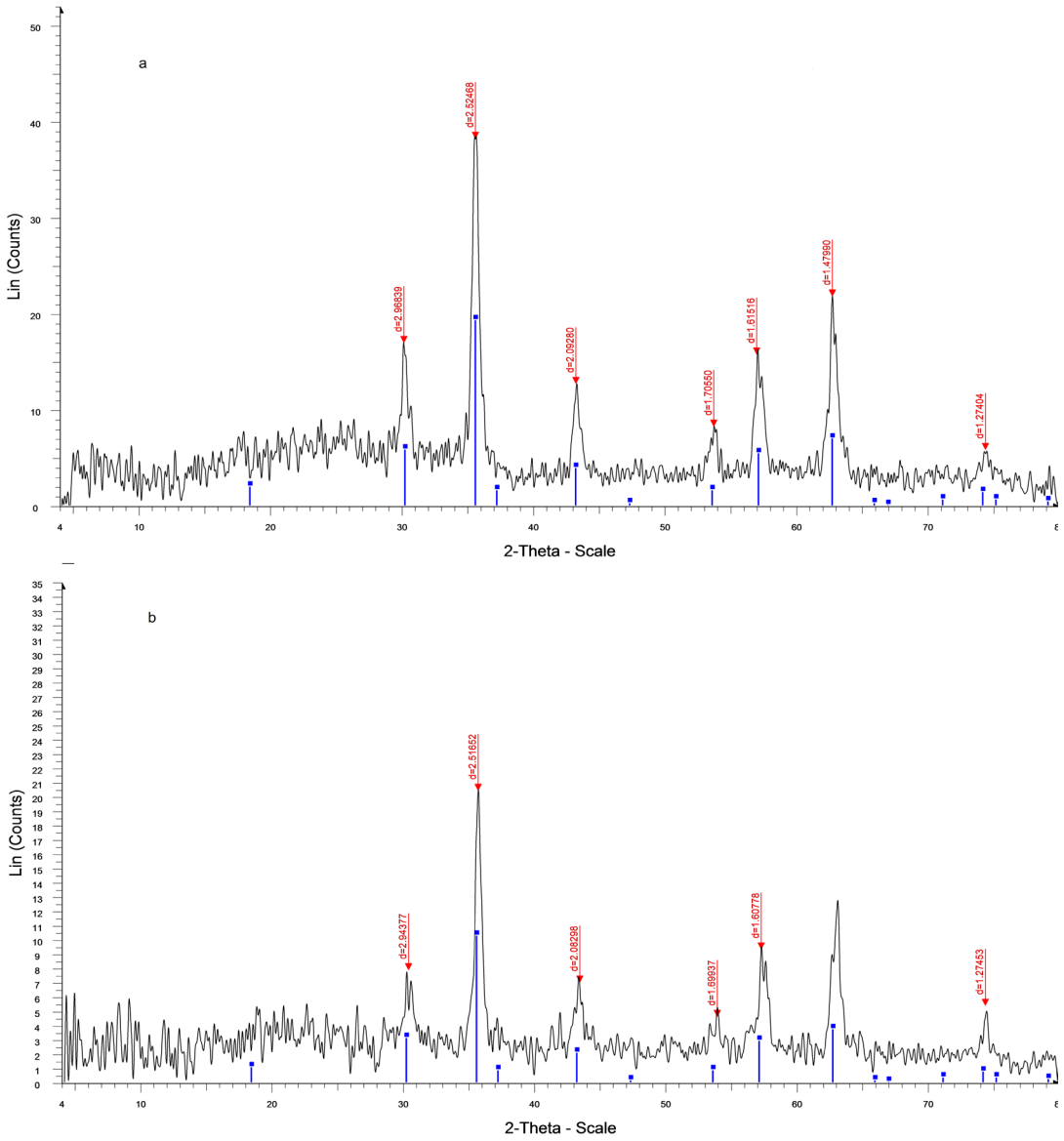


**Fig. 4. XRD spectra of (a) magnetite nanoparticles and (b) iron-loaded magnetite nanoparticles.**

and 62.9° in Fig.4a were corresponded to (1 1 1), (2 2 0), (311), (4 0 0), (4 2 2), (5 1 1), and (1 0 3) crystal planes, which were well matched with face-centered cubic phase of $Fe_3O_4$ [19,20]. No other impurity peaks could be observed, suggesting high crystal purity of $Fe_3O_4$. On the other hand, all the characteristic peaks of $Fe_3O_4$ were also found in Fig.4b after iron ions adsorption, indicating the unchanged crystalline form in the composite. Noticeably, the peak intensity of $Fe_3O_4$ decreased after iron ions loaded on magnetite iron oxide nanoparticles.

*Morphological analysis by scanning electron microscope (SEM) and energy dispersive analysis (EDX)*

Surface morphologies of the adsorbent were examined using a scanning electron microscope (Model: JSM- 5500 LV; JEOL Ltd -Japan) by using high vacuum mode at the Regional Center of Mycology and Biotechnology, Cairo, Egypt.XRD measurements were carried out using a BRUKER D8 Advnaced Fe target Wavelength 1.54A 40kv 40mA Germany (CentralMetallurgical-Research-Institute-CMRDI-Helwan-Cairo-Egypt).

The shape, size and surface morphology of the magnetic iron oxide nanoparticles were investigated previously. The SEM images (Fig.5a) of the prepared $Fe_3O_4$ nanoparticles show agglomeration of these magnetic nanoparticles. This aggregation was attributed to both magneto

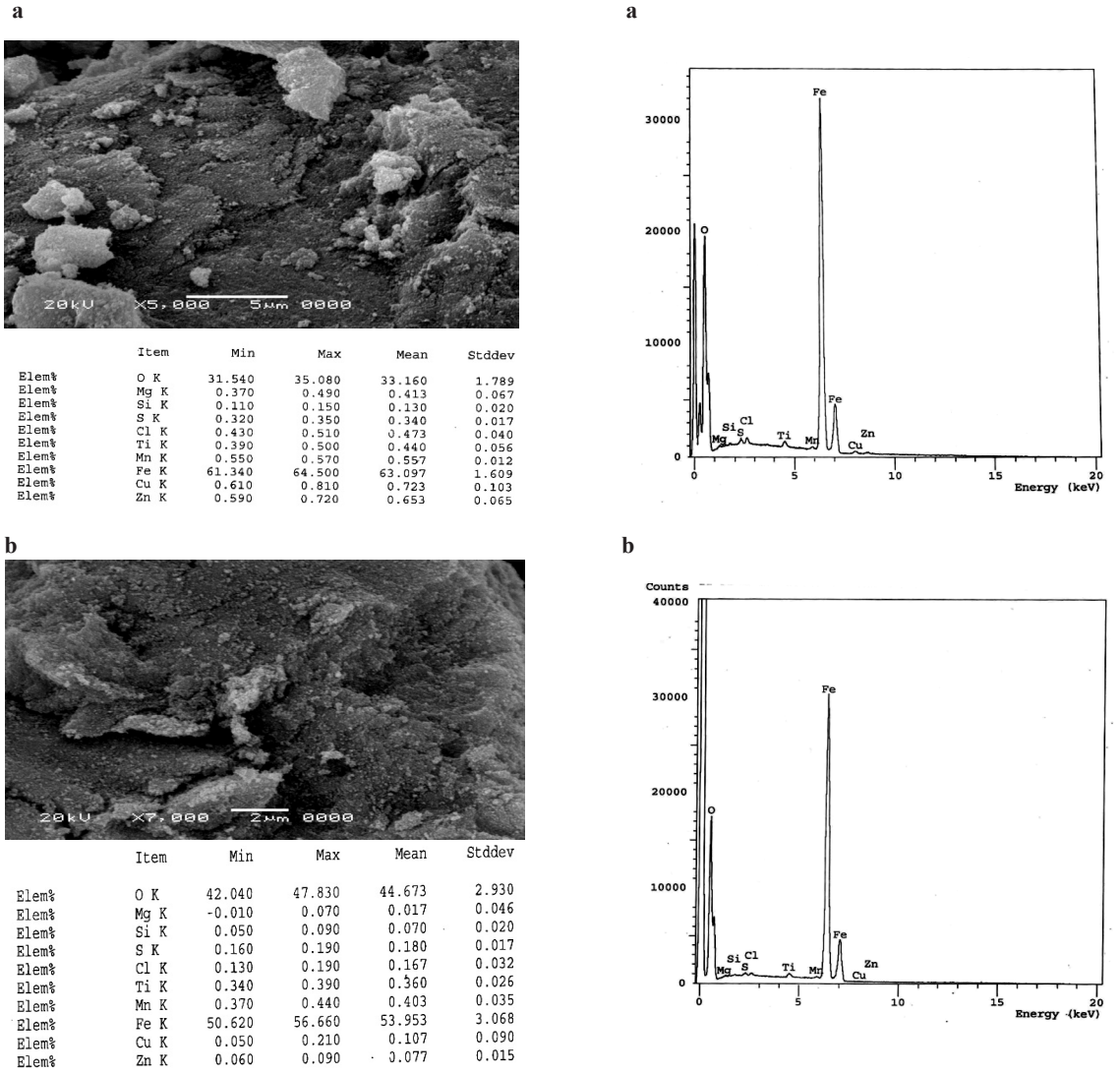


**Fig. 5. SEM-EDX spectra of (a) magnetite nanoparticles, (b) iron ions loaded on magnetite iron oxide nanoparticles.**

dipoles and Van der Wall forces. Generally, the aggregates are smaller than a few microns. SEM elemental mapping clearly shows the iron and oxygen distributed in the $Fe_2O_3$ nanoparticles. Elemental mapping also confirmed the loading of iron, (Fig.5 a and b), on magnetite nanoparticles. Intense iron EDX peaks confirm their adsorption on magnetite surfaces. On the other hand, it was clearly found that primordial Fe-$Fe_2O_4$ had widely distributed pore size from (10 to 20µm), which might give significant contributions in the adsorption process.

*Adsorption experiments*

The adsorption experiments of Fe ions on magnetic iron oxide nanoparticle were conducted in a batch method, which permits complete evaluation of parameters that influence the adsorption process. In this method a fixed amount of magnetic iron oxide nanoparticles was mixed continuously with a specific volume of synthetic solution and groundwater, and continuously agitated at 303K using an incubator shaker at 70rpm, until the equilibrium is reached.

For adsorption studies, a series of 100ml glass flasks were filled with 50ml of metal ion solution of varying concentrations, maintained at required temperature. Then an equal amount of magnetic iron oxide nanoparticles (0.22g) was added to each flask and subjected to agitation for 210min. The resultant solution was centrifuged and the supernatant liquid was subjected for the determination of iron ions using an atomic absorption spectrometry (UNICAM 929 AA Spectrometer, Solar) at DesertResearch Center, Cairo, Egypt.

The adsorption capacities were then obtained by mass balance equation as follows,

$$q_e = \frac{(C_o - C_e)V}{W \times 1000} \quad \text{.....} \quad (2)$$

The removal percentage **yield** (R %) was calculated by the following equation:

$$(R\,\%) = \frac{C_o - C_e}{C_o} \times 100 \quad \text{----------} \quad (3)$$

where $C_o$ and $C_e$ are initial and equilibrium metal ion concentrations in solution, $V$ is the solution volume (L) and $W$ is the amount of dry adsorbent used (g).

## Results and Discussion

*Adsorption process*

*Effect of solution pH on the removal process*

The removal of Fe(III) by the magnetic iron oxide nanoparticles is affected by the pH of the solution. The relationship between the pH of Fe(III) ions solution and the removal percentage (%) at different pH (1-4) for concentration (290.39mg/L) at different times for an adsorbent dose (0.22g) of the magnetic iron oxide nanoparticles at room temperature is illustrated in Fig.6. Effect of the solution pH on the removal percentage of Fe(III)is clearly seen that the iron removal rate of magnetic iron oxide nanoparticles increases gradually with an increasing solution pH from 30.77% at pH 1.67 to 40.39 % at pH 4. This is due to the deprotonation that occurred at the surface of the magnetic iron oxide nanoparticles which creates a strong attractive force between the sorbent surface and the Fe(III) ions. At pH above 4, adsorption experiments were not conducted because of the formation of $Fe(OH)_3$ precipitation.

*Effect of the sorbent dosage on the removal process*

The sorbent dosage strongly affects the metal removal efficiency of a system. The relationship

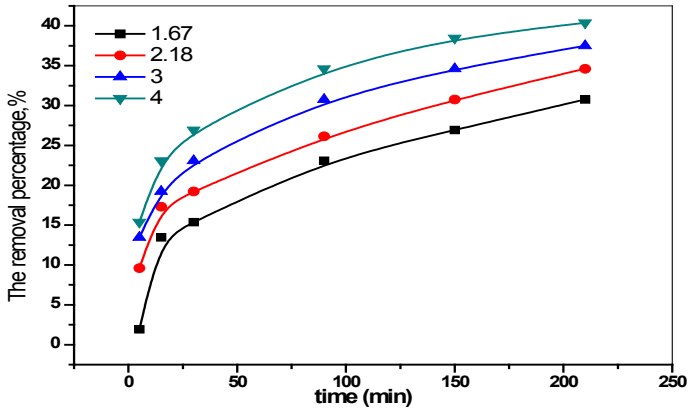


**Fig. 6. Effect of the solution pH on the removal percentage of Fe(III) at interval times.**

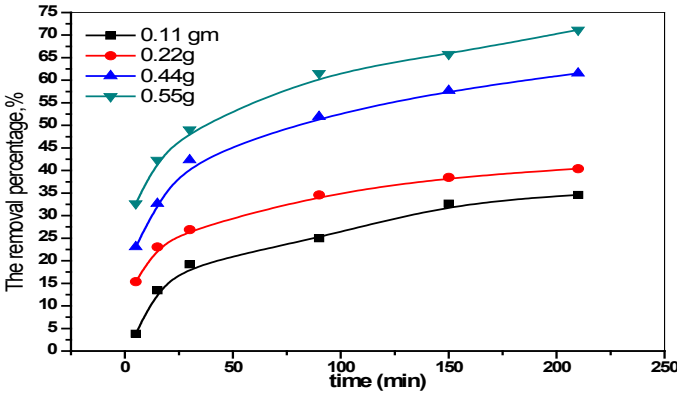


**Fig. 7. Effect of the sorbent dosage on the removal percentage of Fe(III) at interval times.**

between the sorbent dosage (0.11 to 0.55g) of the magnetic iron oxide nanoparticles and the removal percentage (%) at different times for an initial concentration (290.394mg/L) at room temperature and pH 4 is illustrated in Fig.7. It is obvious from this figure that the removal percentages of Fe(III) increased with the dose increase from 0.11 to 0.55g of the magnetic iron oxide nanoparticles.

On other words, when the magnetic iron oxide nanoparticles dosage increased, the removal percentage increased, this is due to the greater surface and availability of more adsorption sites at higher dosages of the adsorbent.

By continuous increasing for the metal uptake (i.e., the amount of metal adsorbed per unit mass of the magnetic ferric oxide nanoparticles), the removal percentage will be decreased. The decrease in metal uptake thereafter may be attributed to the unsaturation/partial filling of sorption sites as the number of sorption sites increased with an increase in the magnetic ferric oxide nanoparticles content, but the amount of sorbet remained constant (i.e., the magnetic ferric oxide nanoparticles has not reached its adsorption capacity) [21].

*Effect of contact time on the removal process*

There is strong relation between the contact time and the removal percentage (%) for a metal ion by a sorbent. The relationship between the contact time (5-210min) and the removal percentage (%) for a sorbent dosage (0.22g) of the magnetic iron oxide nanoparticles at different times for an initial concentration (290.4mg/L) at room temperature and pH 4 is illustrated in Fig.8. It is apparent that as contact time increases, the removal efficiency increases significantly until a plateau is reached to 210min at which the removal efficiency (%) hardly changes with time. The initial sudden increase in removal percentage (%) can be explained in terms of the high driving force adsorption process at the beginning. However, with the increase of the time the driving force decreases as the metal ions being attracted. In addition the available sites on the magnetic iron oxide nanoparticles begin to decrease with time.

*Effect of temperature on the removal process*

During the sorption process, temperature is considered as an important factor for metal adsorption. The effect of temperature on Fe(III) adsorption was studied in 25–60°C under the reaction condition for a 0.22g magnetic iron oxide nanoparticles with concentration of Fe(III) 290.394 mg/L at pH 4 and different times. Figure 9 shows that higher temperature resulted in higher adsorption capacity. When the temperature increased from 25°C to 60°C, the removal percentage (%) increased from 40 to 90%for Fe(III), respectively. Previous studies reported that higher temperature could enhance adsorption due to the increase in surface activity and kinetic energy of the solute [22].

*Effect of the initial metal ion concentration on the removal process*

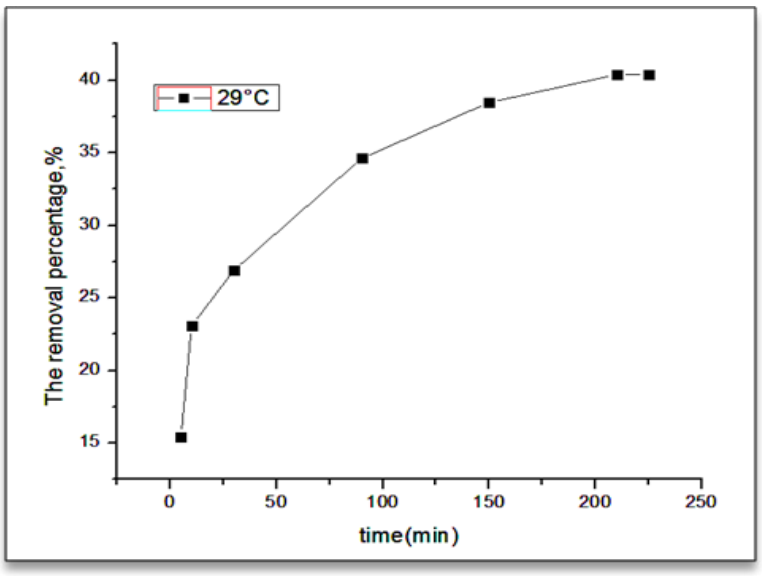


**Fig. 8. Effect of the contact time on the Fe(III) uptake process.**

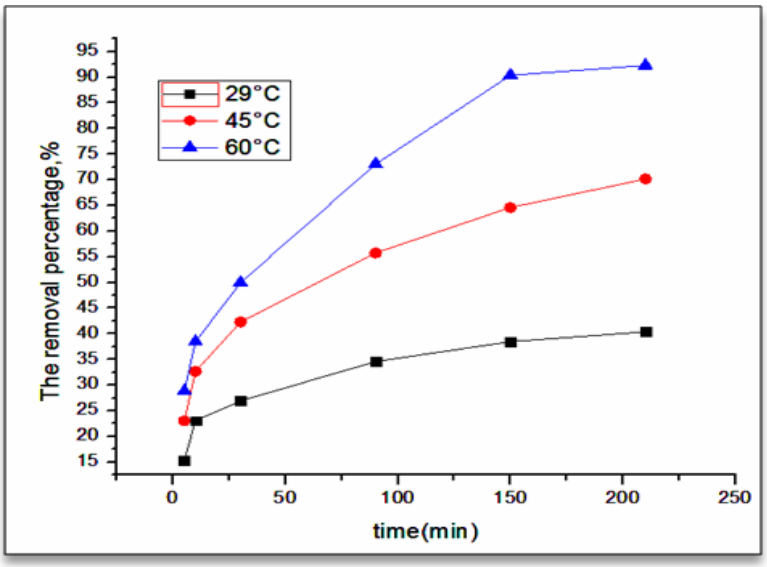


**Fig. 9. Effect of the solution temperature on the Fe(III) uptake process.**

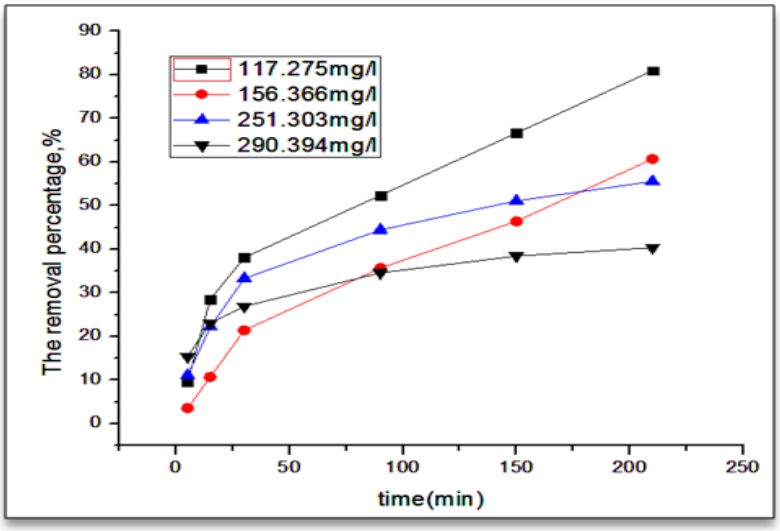


**Fig. 10. Effect of the initial concentration on the Fe(III) uptake process at interval times.**

The initial metal ion concentration constitutes a significant driving force, allowing the ionic mass transfer between the aqueous and the solid phase. The relationship between initial Fe(III) concentration (117.275 - 290.4mg/L) and the removal percentage (%) at different times for an adsorbent dose (0.22g) of the magnetic ferric oxide nanoparticles at room temperature and pH 4 is illustrated in Fig.10. From this figure, it is noticed that the removal percentage (%) of Fe(III) increases with the initial concentration decrease until reaches to the best concentration 117.275mg/L, this is due to the concentration gradient developed at the solid/solution interface.

At higher concentration of metal ions, the active sites of the magnetic ferric oxide nanoparticles well be saturated by the metal ions and the process of adsorption decrease, while at low concentrations occurred an attraction between the metal ions and the sorbent at the surface by some attractive forces that leading to an increase in the the removal percentage (%).

In other words, an increase in initial metal ion concentration results in a decrease in the amount of metal ions removal efficiency, i.e.,

the percentage of adsorption decreases. It can be concluded that the rate of binding of Fe(III) ions with the active sites of the magnetic ferric oxide nanoparticles is initially high, but it gradually decreases to reach equilibrium. This suggests that the removal process is highly concentration dependent. At lower concentrations, the number of metal ions which are available in the solution is less as compared to the available sites on the adsorbent. However, at higher concentrations the available sites for adsorption become fewer and the removal percentage efficiency of metal ions decreases. [23]

## Results and Discussion

*Adsorption kinetics of the metal ions*

In order to analyze the adsorption mechanism of heavy metal ions (Fe) onto the magnetic iron oxide nanoparticles, three kinetic models including the pseudo-first-order, the pseudo-second-order and the intra-particle diffusion models were applied to fit the experimental data obtained at three different temperatures for the heavy metal ion solution.

*Pseudo-first order equation (Lagergren, 1898)*

The pseudo-first order equation of Lagergren, 1898 [24] is generally expressed as follows:

$$\frac{dq}{dt} = k_1(q_e - q_t) \quad \text{----------(4)}$$

Where $q_e$ and $q_t$ is the amount of metal sorbed per unit weight of sorbent at equilibrium and at any time t, respectively (mg/g) and $k_1$ is the rate constant of pseudo-first order sorption ($min^{-1}$). After integration and applying boundary conditions, for $q = 0$ , $t = 0$ , the integrated form of Eq. (4) becomes.

$$\ln(q_e - q_t) = \ln q_{e,1,cal} - k_1 t \quad \text{----------} \quad \textbf{(5)}$$

The values of rate constant $(k_1)$ and equilibrium capacity $(q_1(e,1,cal))$ can be obtained from the slope and intercept of plotting $\ln(q_e - q_t)$ against time for three temperatures (Fig.11).

*Pseudo-second order equation(Ho and Mckay, 1998)*

If the rate of sorption is a second order mechanism according to Ho and Mckay,1998 [25], the pseudo-second order chemisorption kinetic rate equation is expressed as;

$$\frac{dq}{dt} = k_2(q_e - q_t)^2 \quad \text{----------} \quad \textbf{(6)}$$

Where $k_2$ the rate is constant of pseudo-second order sorption $\left(gmmmol^{-1}\,min^{-1}\right)$, is the amount of soluted sorbate at equilibrium (mg/g) and $q_t$ is the amount of solutessorbets on the surface of the adsorbent at any time $t$ (mg/g). Integrating the equation (6) for the boundary conditions for $t = 0$, $q = 0$ gives the following equations (7 and 8);

$$\frac{t}{q} = \frac{1}{k_2 q_{e,2}^2} + \frac{1}{q_{e,2}} t \quad \text{----------(7)}$$

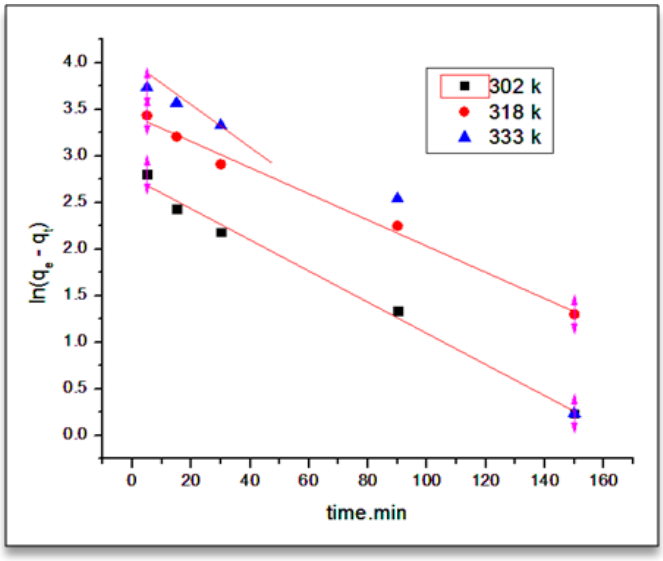


**Fig. 11. The pseudo-first order model at different temperature.**

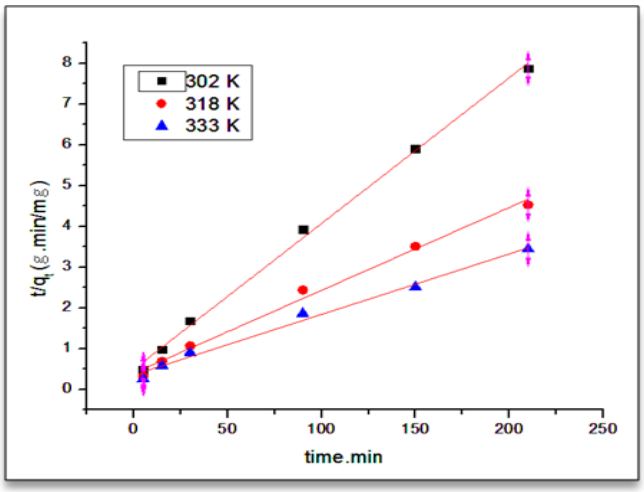


**Fig. 12. The pseudo-second order modelat different temperature.**

And

$$h = k_2 q_{e,2}^2 \text{ ---------- (8)}$$

Where $h\left(\mathbf{mgg^{-1}\,min^{-1}}\right)$ means the initial adsorption rate, and the constants can be determined experimentally by plotting of $t/q$ against $t$ (Fig.12).

The slope and the intercept of each linear plot (Fig.11 and 12) are used to calculate the adsorption rate constants ($k_1$ and $k_2$) and the amount of adsorption in equilibrium ($q_e$). The calculated kinetic parameters for adsorption of iron ions (Fe) onto a linear form at two initial concentrations of iron ions (low and high) are listed in Table 2. As can be observed, at all temperatures (29$^0$C, 45$^0$C and 60$^0$C) of Fe ions, the correlation coefficient ($R^2$) of the pseudo-second-order kinetics model is higher than that of the pseudo-first-order kinetic model. The consistency of the experimental data with the pseudo-second-order kinetic model indicates that the adsorption of Fe ions onto the magnetic iron oxide nanoparticles at low temperature is controlled by chemical adsorption (chemisorption) involving valence forces through sharing or exchange electrons between sorbent and sorbate. In chemical adsorption, it is assumed that the adsorption capacity is proportional to the number of active sites occupied on the adsorbent surface [26].

*Intra-particle diffusion model (Weber and Morris, 1963)*

The initial rate of the intraparticle diffusion according to Weber and Morris, 1963 [27] is the

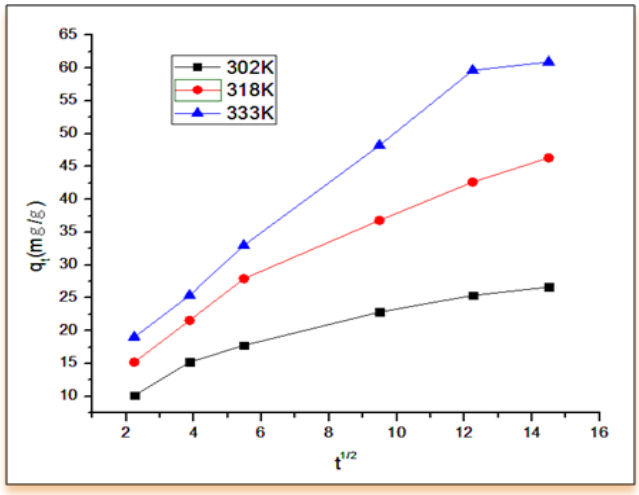


**Fig. 13. intra-particle diffusion model at different temperature.**

following:

$$q_t = K_i t^{0.5} + C \quad \text{----------(9)}$$

Where $K_i$ is the intraparticle diffusion rate coefficient $(\mathbf{mg\ g^{\uparrow}(-1)\ min^{\uparrow}(-0.5)})$ and $C(\mathbf{mg\ g^{-1}})$ provides an idea about the thickness of the boundary layer[24]. The $K_i$ and $C$ can be obtained from the slope and intercept of a straight line plot of $q_t$ versus $t^{0.5}$ (Fig.13).

The kinetic results were analyzed by the intra-particle diffusion model in order to elucidate the diffusion mechanism. The intra-particle diffusion model parameters for adsorption of iron ions onto the magnetic iron oxide nanoparticles at three temperatures (29$^0$C, 45$^0$C and 60$^0$C) were calculated as listed in Table 2. According to this model, if the plot of $q_t$ versus $t^{1/2}$ gives a straight line, then intra-particle diffusion is involved in the adsorption process and if this line passes through the origin then intra-particle diffusion is the rate-controlling step. However, if the data present multi-linear plots, then two or more steps influence the adsorption process such as external diffusion, intra-particle diffusion and etc…..

As can be observed, at a low initial concentration of iron ions, the data points are related by two straight lines. The first sharper portion is attributed to the diffusion of adsorbate through the solution to the external surface of the adsorbent (external diffusion) and the second portion describes the gradual adsorption stage, corresponding to the diffusion of adsorbate molecules inside the pores of the adsorbent (intra-particle diffusion). At high initial concentrations, the data points are related by one straight line, indicating that intra-particle diffusion is mainly involved in the adsorption process. The deviation of straight lines from the origin indicates that the intra-particle diffusion is not the sole rate-controlling mechanism.

**TABLE 2. Kinetic parameters &temperature [29$^0$C (302K), 45$^0$C (318K), 60$^0$C (333K)].**

| Temp (K) | Pseudo-first order | | | Pseudo-second order | | | | Intrapaparticle diffusion | | |
|---|---|---|---|---|---|---|---|---|---|---|
| | $q_{e,1,cal}$ | $k_1$ | $R^2$ | $q_{e,2,cal}$ | $k_2$ | H | $R^2$ | $K_{int}$ | C | $R^2$ |
| **302** | 15.958 | 0.017 | 0.989 | 27.964 | 0.003 | 1.991 | 0.997 | 1.28 | 9.475 | 0.936 |
| **318** | 31.118 | 0.014 | 0.989 | 49.213 | 0.001 | 2.465 | 0.99 | 2.48 | 11.98 | 0.975 |
| **333** | 55.119 | 0.023 | 0.919 | 67.385 | 0.001 | 2.763 | 0.988 | 3.618 | 12.21 | 0.976 |

The obtained results demonstrate that, the kinetics of adsorption vary with the temperature of heavy metal ion solutions. At all the studied temperatures, adsorption of Fe(III) is controlled by chemical adsorption, external diffusion and to some extent intra-particle diffusion (low $R^2$ values). This can be explained by the fact that at higher temperature, the mass transfer driving force is larger, and hence this resulted high diffusion rates of heavy metal ions within the pores of the magnetic iron oxide nanoparticles [28].

*Adsorption isotherm modeling of the ions.*

Isotherms are the equilibrium relations between the concentration of adsorbate on the solid phase and its concentration in the liquid phase. From the isotherms, the maximum adsorption capacity can be obtained. These data provide information on the capacity of the sorbent or the amount required to remove a unit mass of pollutants under the system conditions. The data has been subjected to different adsorption isotherms. Langmuir [29], Freundlich [31], Temkin [32] and D-R [33] models are the most common isotherms describing solid–liquid adsorption system.

Adsorption isotherm experiments were also performed by agitating an amount of the magnetic iron oxide nanoparticles with a 50ml aqueous solution at varies metal ion concentrations and interval times. The contents were continuously agitated in a temperature controlled flask shaker. At the end of the pre-determined time intervals. The amount adsorbed was determined from the difference in the initial and residual concentrations of the metal ion in the liquid phase. The data were

fitted into the following isotherms.

*Langmuir isotherm*

Langmuir isotherm [29] is often used to describe adsorption of solute from liquid solutions on adsorbent and this model assumes monolayer adsorption onto a homogeneous surface with a finite number of identified sites. In order to know the feasibility of the isotherm, the essential features of the Langmuir model can be expressed in terms of separation factor or equilibrium parameter $R_L$.

The Langmuir equation is represented in the linear form as follows:

$$\frac{C_e}{q_e} = \frac{1}{K_L Q_{max}} + \frac{C_e}{Q_{max}} \text{----------(10)}$$

Where $C_e$ is the equilibrium concentration of adsorbate (mg/l), $q_e$ is the amount of soluted sorbate at equilibrium (mg/l), $K_L$ is the Langmuir adsorption constant (L $mmol^{-1}$) which is related to the affinity of the binding sites, and $Q_{max}$ is the theoretical maximum adsorption capacity (mg/g).

Langmuir plots $\left(\frac{C_e}{q_e} \; vs. C_e\right)$ for adsorption of metal ions onto magnetic iron oxide nanoparticles at different concentrations and interval times.

For the Langmuir isotherm model, a dimensionless constant $(R_L)$, commonly known as separation factor or equilibrium parameter can be used to describe the favorability of adsorption on the polymer surface by:

$$R_L = \frac{1}{1 + K_L C_0} \text{ ---------- (11)}$$

Where $C_0$ is the initial metal ion concentration and $K_L$ is the Langmuir equilibrium constant.

The values of $R_L$ indicate that the shapes of isotherms to be either unfavorable ($R_L > 1$), linear ($R_L = 1$), favorable ($0 < R_L < 1$) or irreversible ($R_L = 0$). The $R_L$ values for Fe ions were calculated and plotted against the initial metal ion concentration. It is observed from Fig.14 that, the sorption of Fe ions on the magnetic iron oxide nanoparticles increases as the initial metal ion concentration increase, indicating that this adsorption is even favorable for Fe ions ion concentrations that have been investigated [30]. It is noticed that $R_L$ values in this study are in the order ($0 < R_L < 1$) indicated that the magnetic iron oxide nanoparticles are a suitable adsorbent for the adsorption of Fe(III) ions from aqueous solutions.

The Freundlich isotherm is derived by assuming a heterogeneous surface with a non-uniform distribution of sorption heat over the surface. It can be stated in the linear form as follows:

$$\ln q_e = \ln K_F + \frac{1}{n} \ln C_e \text{ ---------- (12)}$$

Where $K_F$ (mg $g^{-1}$) and $n$ are isotherm constants indicate the capacity and intensity of the adsorption, respectively.

The linear plot between $lnq_e$ verses $lnC_e$ gives a slope which is equal to the value of $1/n$ and the intercept is $lnK_f$. The magnitude of $1/n < 1$ indicates the favorability of a process of adsorption.

Freundlich isotherm represents the relationship

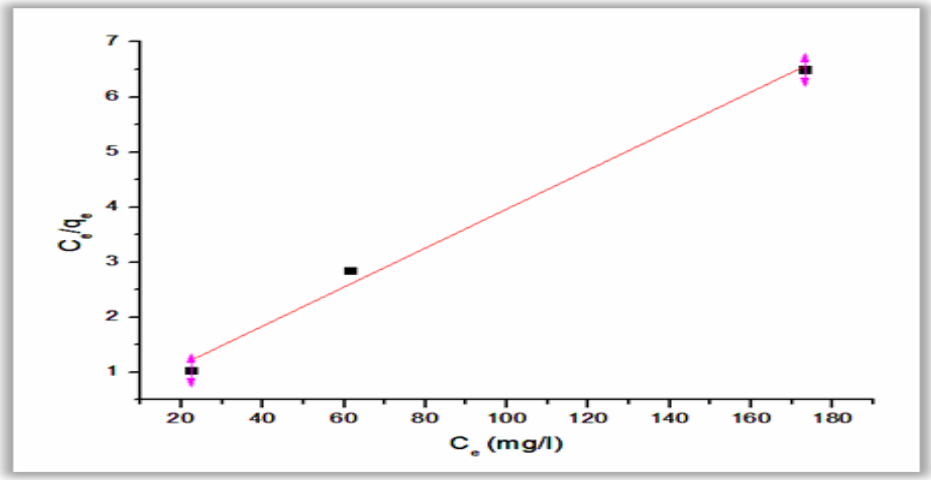


**Fig. 14. Langmuir isotherm plot Freundlich Adsorption Isotherm [31].**

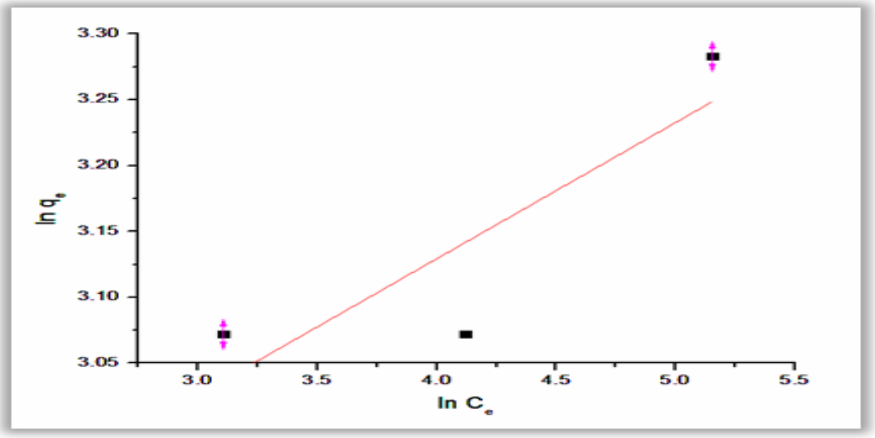


**Fig. 15. Freundlich adsorption isotherm plot The Temkin Isotherm [32].**

between the amounts of ionic species exchanged per unit mass of magnetic iron oxide nanoparticles ($q_e$) and the concentration of the ionic species at equilibrium ($C_e$). It is obvious from Fig.15 that, the uptake is nearly constant and then rapidly increased with increase in the initial concentration, this may be due to that at lower concentration of the solute in the solution leads to low adsorption where at increase the solute concentration, the adsorption process will increase due to the abundances of the Fe ions in the solution. On the other hand, the irregularity of this adsorption indicates that removal of Fe iron by magnetic iron oxide nanoparticles does not obey the freundlich isotherm model.

The Temkin isotherm has been used in the following form:

$$q_e = \left(\frac{RT}{b_T}\right)\ln A_T + \left(\frac{RT}{b_T}\right)\ln C_e \text{----------(13)}$$

Where $B_T$ $B_T = \left(\frac{RT}{b_T}\right)$ is the Temkin constant (J/mol) related to adsorption heat, $T$ is the absolute temperature$R$ $(K)$ is the gas constant (8.314 J/mol K), and $A_T$ is the Temkin isotherm constant (L/g). ($B_T$) and ($A_T$) can be calculated from the slopes ($B_T$) and intercepts $(B]_T \ln[A_T)$ of the plot of $q_e$ verses ln $C_e$.

Temkin isotherm assumes that (i) the heat of adsorption of all the molecules in a layer decreases linearly due to the adsorbent–adsorbate interactions and (ii) adsorption is characterized by a uniform distribution of binding energies, to up some maximum binding energy. A plot of $q_e$ versus ln$C_e$ enables the determination of the isotherm constants $B_T$ and $A_T$ from the slope and the intercept (Fig.16), respectively. Temkin isotherm parameters have also been listed in Table 3. $A_T$ value for Fe ions was 185.65L/min, suggesting strong bonding between the magnetic iron oxide nanoparticles and the metal ion at experimental condition. The $B_T$ values or heat of adsorption for iron was 2.49J/Mol (Table 3).

**TABLE 3. Isotherm parameters.**

| **Freundlich** | | | **Langmuir** | | | |
|---|---|---|---|---|---|---|
| 1/n | $K_F$ (mg/g) | $R^2$ | $Q_{max}$ (mg/g) | $K_L$ (L/mg) | $R_L$ | $R^2$ |
| 0.103 | 15.114 | 0.512 | 28.225 | 0.0832 | 0.093<br>0.0713<br>0.0397 | 0.987 |
| **D-R** | | | | **Temkin** | | |
| B ($mol^2/kJ^2$) | $X_{D-R}$ (mg/g) | E(kJ/mol) | $R^2$ | $A_T$ (L/min) | $R^2$ | BT |
| $1.16x10^{-05}$ | 24.39 | 207.71 | 0.2974 | 185.65 | 0.5167 | 2.489 |

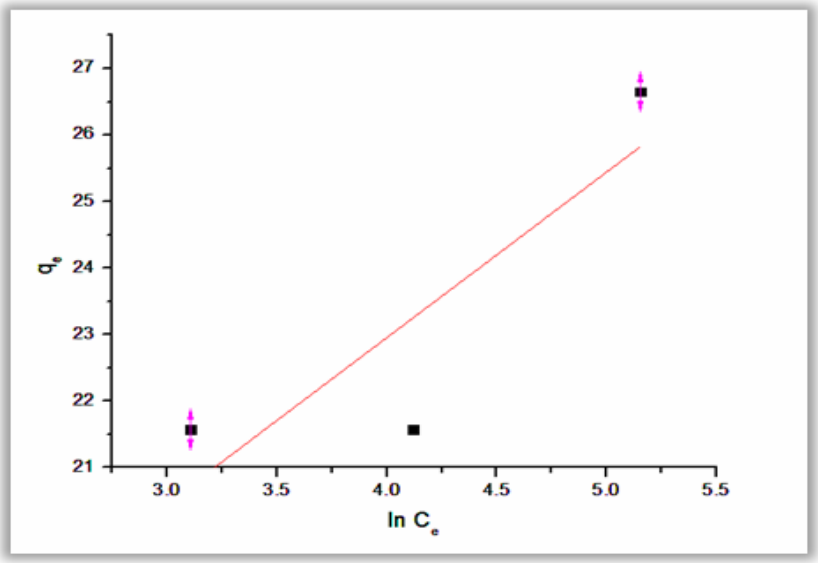


**Fig. 16. Temkin isotherm plot.**

It is obvious from Fig.16 that, the uptake is nearly constant and then rapidly increased with increase in the initial concentration, this may be due to that at lower concentration of the solute in the solution leads to low adsorption where at increases the solute concentration, the adsorption process will increase due to the abundances of the Fe ions in the solution. Also, the irregularity of this adsorption indicates that removal of Fe iron by magnetic iron oxide nanoparticles does not obey the Temkin isotherm model.

*Dubinin–Radushkevich isotherm model (D-R) [33]*

The linear form of Dubinin and Radushkevich isotherm model equation can be expressed as:

$$\ln q_e = \ln(X_{D-R}) - \beta\varepsilon^2 \text{ ---------- (14)}$$

Where $X_{D-R}$ is the theoretical monolayer saturation capacity (mg $g^{-1}$), $\beta$ is the Dubinin–Radushkevich model constant ($mol^2\ J^{-2}$). $\varepsilon$ is the polanyi potential and is equal to

$$\varepsilon = RT \ln\left(1 + \frac{1}{C_e}\right) \text{ ----------(15)}$$

Where R, T and $C_e$ represent the gas constant (8.314KJ/Mol), absolute temperature (K) and adsorbate equilibrium concentration (mg/L), respectively.

The $X_{D-R}$ and $\beta$ can be calculated from the slopes ($\beta$ ) and intercepts $\ln(X_{D-R})$ of the plot of $(\ln q_e)$ vs$(\varepsilon^2)$at different temperatures for metal ions onto the magnetic iron oxide nanoparticles.

The value of $E_{D-R}$ is related to the sorption means free energy $\left(\frac{KJ}{Mol}\right)$. The relationship is expressed as:

$$E_{D-R} = \frac{1}{\sqrt{-2\beta}} \text{ ---------- (16)}$$

The equilibrium data were examined using the Dubinin–Radushkevick isotherm model in order to determine the nature of the sorption processes as physical or chemical. The Dubinin–Radushkevick sorption isotherm is more general than the Langmuir isotherm as its derivation is not based on the ideal assumption such as equipotency of the sorption sites, absence of stoic hindrance between sorbed and incoming particles and surface homogeneity on a microscopic level. The Dubinin–Radushkevick equation has been used to determine the mean free energy of sorption.

From Table 3, the mean sorption energy ($E_{D-R}$) was evaluated as 207.71 KJ/Mol for the sorption of Fe ions, onto the magnetic iron oxide nanoparticles. According to the available literature, the $E_{D-R}$ value ranges from 1.0 to 8.0KJ/Mol for physical adsorption and from 8.0 to 16.0KJ/Mol for chemical ion exchange and higher 16.0KJ/Mol for chemical reaction. Therefore, these results indicate that the adsorption of the iron ions onto the magnetic iron oxide nanoparticles might be attributed to chemical ion-exchange mechanism [34].

Figure 17 shows that, the polanyi potential increases with the increase in the uptake of Fe

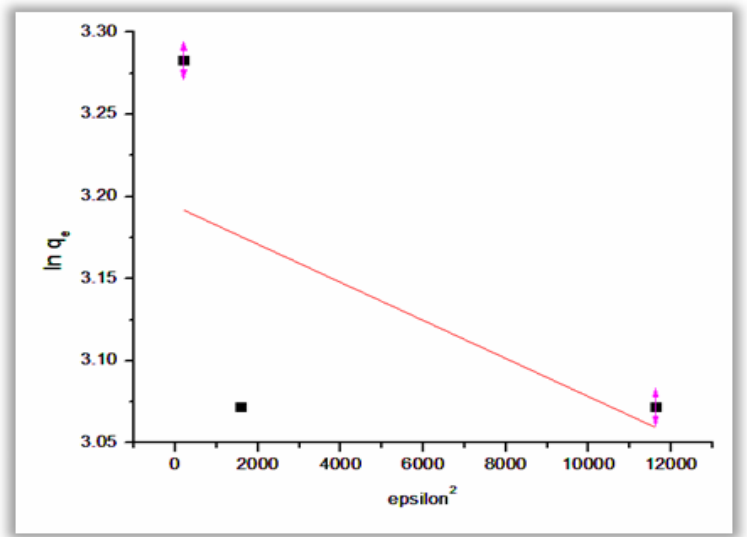


**Fig. 17. Dubinin–Radushkevich isotherm model plot.**

ions onto magnetic iron oxide nanoparticles, indicating a chemical sorption.

The adsorption parameters obtained from both the models were given in Table 3. The experimental data for Fe ions were fitted well with Langmuir isotherm suggesting that the metal ions sorbed from monolayer coverage on the adsorbent surface. The correlation co-efficient ($R^2$) value found to be equal to 0.987 indicates that the metal ions can be described by the Langmuir isotherm.

*Thermodynamic studies*

The thermodynamic parameters such as free energy change ($\Delta G$), enthalpy changes ($\Delta H$) and entropy change ($\Delta S$) were obtained from the gibbs free energy and van't Hoff equation.

The sorption data obtained from the above study (as the effect of sorption process temperature) was used to calculate the thermodynamic parameters. The calculated Gibbs free energy change (ΔG), enthalpy change (ΔH) and entropy change (ΔS) values for the sorption process of metal ions by used magnetic iron nanoparticles material.

The Gibbs free energy changes with the temperature and pressure of the thermodynamic system. The van 't Hoff isotherm can be used to determine the Gibbs free energy for non-standard state reactions at a constant temperature.

The Gibbs free energy change, (ΔG), (KJ/Mol) was calculated from the following equation; [35]

$$T\Delta S^o - \Delta H^o = \Delta G^o \quad \text{---------- (17)}$$

The van 't Hoff equation relates the change in the equilibrium constant Kd of a chemical reaction to the change in temperature T given the standard enthalpy change ($\Delta H^o$) for the process. It was proposed by Dutch chemist Jacobus Henricus van 't Hoff in 1884 in his book Études de dynamique chimique (Studies in Dynamic Chemistry), where the van't Hoff equation can be summarized as follows[36-38];

$$\ln K_d = \frac{\Delta S^o}{R} - \frac{\Delta H^o}{RT} \quad \text{---------- (18)}$$

The values of ΔH and ΔS were obtained from the slope $\left(\frac{-(H)}{R}\right)$ and intercept $((S/R)$, respectively, of the plot of $\ln K_d$ Vs. $\frac{1}{T}$.

In order to further support the assertion that physical adsorption is the predominant mechanism, the values of the activation energy $(E_a)$ and sticking probability $(S^*)$ were estimated from the experimental data. They were calculated using a modified Arrhenius type equation related to surface coverage (θ),[39] as expressed in equations:

$$\theta = 1 - \frac{C_e}{C_0} \quad \text{---------- (19)}$$

Where $C_0$ and $C_e$ are the initial and equilibrium metal ion concentrations, respectively

$$S^* = (1-\theta)exp\left(\frac{E_a}{RT}\right) \quad \text{---------- (20)}$$

The sticking probability, $S^*$, is a function of the adsorbate/adsorbent system under consideration and is dependent on the temperature of the system.

The combination of Eqs. (19) and (20) gives the equation (21):

$$\ln \frac{C_e}{C_0} = \ln S^* + \frac{E_a}{RT} \text{----------} \quad (21)$$

The values of $E_a$ and $S^*$ were obtained from the slope $\left(\frac{E_a}{R}\right)$ and intercept $\ln S^*$, respectively, of the plot of $\ln \frac{C_e}{C_0}$ Vs. $\frac{1}{T}$.

The parameter S* indicates the measure of the potential of an adsorbate to remain on the adsorbent indefinitely. It can be expressed as in Table 4. The effect of temperature on the sticking probability was evaluated throughout the temperature range from 302 to 333K by calculating the surface coverage at the various temperatures. Table 4 also indicated that the values of S* ≤ 1 for the adsorbent, hence the sticking probability of the metal ions onto the adsorbent systems are very high.

The values of Δ*H* and Δ*S* were calculated from the slope and intercept of the van't Hoff plots of ln $K_d$ versus 1/*T* (Fig.18). The obtained values of thermodynamic parameters are listed in Table 4. The positive value of enthalpy Δ*H* is indicates that the adsorption process is endothermic and the binding between the solute and the adsorbent is strong. Moreover, the magnitude of Δ*H* can provide information about adsorption which belongs to phyisosorption (2.1–20.9 KJ/Mol) or chemisorption (80–200 KJ/Mol) [40]. also, the positive value of Δ*S*° revealed that there are some structural changes in the magnetic iron oxide nanoparticles and also reflect the affinity of the

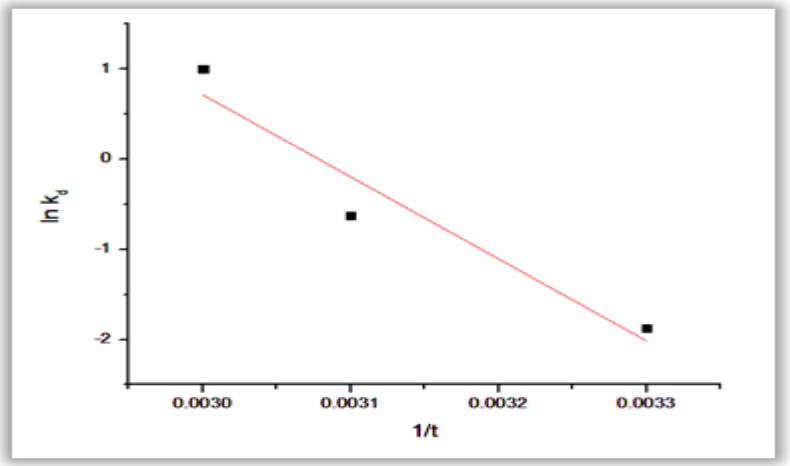


**Fig. 18.Van't Hoff equation model plot.**

**TABLE 4. Thermodynamic parameters.**

| Temp. | ΔG⁰ KJ/Mol | ΔH⁰ KJ/Mol | ΔS⁰ J/mol K | $R^2$ | S* | Ea KJ/Mol | $R^2$ |
|---|---|---|---|---|---|---|---|
| 302<br>318<br>333 | 5.315<br>1.588<br>-1.906 | 75.67 | 232.959 | 0.861 | $5.63 \times 10^{-10}$ | 52.717 | 0.732 |

magnetic iron oxide nanoparticles for adsorping Fe(III). In addition the positive values of Δ*G*° (5.315 and 1.588) at 302K and 318K designated the degree of no spontaneity of the adsorption process, while at 333K the negative Δ*G*° value (-1.906) showed that the adsorption was more favorable at high temperature for Fe(III) [41].

In order to further support the assertion that the adsorption is the predominant mechanism, the values of the activation energy (Ea) and sticking probability (S*) were estimated from the experimental data. They were calculated using a modified Arrhenius type equation related to surface coverage. The sticking probability, S*, is a function of the adsorbate/adsorbent system under consideration and is dependent on the temperature of the system. The parameter S* indicates the measure of the potential of an adsorbate to remain on the adsorbent indefinitely. It can be expressed as in Table 4. The effect of temperature on the

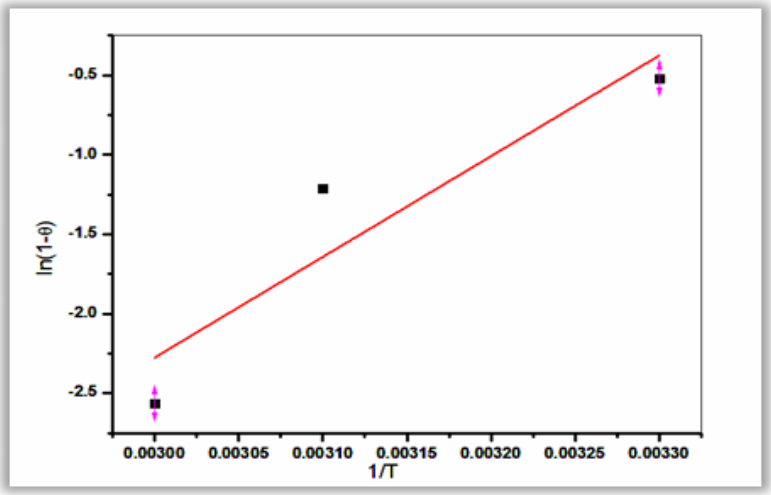


**Fig. 19. Sticking probability plot of Fe(III) adsorption.**

sticking probability was evaluated throughout the temperature range from 302 to 333 K by calculating the surface coverage at the various temperatures (Fig.19). Table 4 also indicated that the values of $S^* \leq 1$ for the adsorbent, hence the sticking probability of the Iron ions onto the adsorbent systems are very high.

*Sorption activation energy*

According to Arrhenius equation, activation energy of the adsorption ($E_a$, KJ/Mol) can be calculated using the above equation. The magnitude of activation energy gives an idea about the type of adsorption which is mainly physical or chemical. Low activation energies (<40 KJ/Mol) are characteristics for physical adsorption, while higher activation energies (>40 KJ/Mol) suggest chemical adsorption [42]. According to activation energy obtained for the adsorption of Fe(III) was 52.717 KJ/Mol indicates that the adsorption process is chemisorption.

*Applications of magnetic iron oxide .4.5 nanoparticles ($Fe_3O_4$) in groundwater treatment at El-Sadat area*

Real water systems as the groundwater in El-Sadat area contain multiple ions. Therefore, competition for adsorption sites by magnetic iron oxide nanoparticles affects the overall sorption efficiency of the adsorbent. Thus, the efficiency of the adsorbent in the real water system toward Fe(III) ions in groundwater samples collected from El-Sadat City, El-Monofia governorate, Egypt was investigated. Selected physicochemical parameters of the selected groundwater samples are given in Table 1. Magnetic $Fe_3O_4$ nanoparticles were used to remove Fe(III) ions from this water under the experimental conditions obtained from batch sorption studies. A $Fe_3O_4$ nanoparticles dose of 0.22g was added to 100mL

**TABLE 5. Iron ions removal from contaminated groundwater sample using $Fe_3O_4$ nanoparticles.**

| Ion | Initial concentration (ppm) | Final concentration (ppm) | % |
|---|---|---|---|
| Fe(III) | 2.8 | 1.130 | 59.64 |

sample. After equilibrating 210min at room temperature, the samples were filtered and the metal ion concentrations were determined using spectroscopic technique AAS. The concentrations before and after the removal metal ion are presented in Table 5. It is clear that the final the Fe(III) metal ion concentrations were reduced.

A magnetic iron oxide($Fe_3O_4$) nanoparticle was easily manipulated by a low strength external magnetic field, permitting easy recovery from groundwater. Therefore, magnetic $Fe_3O_4$ nanoparticles can be utilized for iron(III) ions removal from contaminated water more than once, where these impurities may cause adsorbent

fouling and require frequent regeneration. Simple separation by a magnetic field would allow easy recovery of the used paramagnetic $Fe_3O_4$ nanoparticles, followed by redispersion. Thus, this adsorbent might be used as readily available low cost sustainable adsorbent for iron(III) removal.

*Summary and conclusion*

El-Sadat City is one of the newly constructed industrial settlements in the western desert fringes surrounding the Nile Delta. Groundwater is the only source of drinking water, as well as for domestic, industrial and agricultural purposes. Over-exploitation of the groundwater to meet all the potential needs could facilitate the migration of the accumulated pollutant to reach the underlying groundwater. Contamination of groundwater due to different activities could therefore severely endanger survival in this harsh environment. The occurrence of heavy metals in industrial and municipal sewage effluents is of interest because they are often present at significant levels and if infiltrated to groundwater can have severe effects on public health.

Magnetic iron oxide nanoparticles were synthesized by co-precipitation method. Adsorption properties of the synthesized magnetic iron oxide nanoparticles towards iron ions were systematically investigated, including pH effect, adsorbent dosage, initial concentration, temperature, adsorption equilibrium and adsorption kinetics. The adsorption kinetics was studied by the pseudo fisrt-order and pseudo second-order models. The adsorption isotherm for the removed iron ions was described by the Langmuir, Freundlich, D-R and Temkin isotherm models. The obtained results reveled that, the maximum adsorption capacity for Fe ions was 28.225mg/g and the removal percentage reached nearly 85% at adsorbent dosage 0.22g, temp. 600C, time 210min., pH 4 and initial concentration 117.275mg/L. The adsorption capacity was increased with the increase of temperature and decrease of adsorbent dosage. The reaction obeyed both the pseudo second-order model and Langmuir isotherm model (with correlating constant R2 is 0.98). Also, the calculated mean free energy of the sorption from the Dubinin–Radushkevich isotherm was found to be 207.71KJ/Mol for iron ions, indicating a chemical sorption. With high regression coefficients for Fe ions at 302K., and thermodynamic calculations suggested that the adsorption of iron ions onto the magnetic iron oxide nanoparticles is an endothermic process.

**References**


1. Bánfalvi, G., "Heavy Metals, Trace Elements and their Cellular Effects". In Bánfalvi, G. *Cellular Effects of Heavy Metals*. Springer. pp. 3–28. ISBN 9789400704275(2011).

2. Duruibe J.O., Ogwuegbu M.O.C. and Egwurugwu J.N., Heavy metal pollution and human biotoxic effects. *International Journal of Physical Sciences*. **2**(5), 112-118 (2007).

3. Akpor, O.B. and Muchie, M., Remediation of heavy metals in drinking water and wastewater treatment systems: Processes and applications. *International Journal of the Physical Sciences,* **5**(12), 1807-1817(2010).

4. Green W.F., Hall J.O. and Bonagura J.D., *Iron Toxicities, in Kirk's Current Therapy XII Small Animal Practice*, W.B. Saunders Co.(Saunders academic publisher), Philadelphia, U.S.A., 240-242 (1995).

5. Health and Welfare Canada, Nutrition recommendations, *The Report of the Scientific Review Committee 1990.* Ottawa: Canadian Government Publishing Centre, 1-206 (1990).

6. Gu H., Zhang H., Ma C., Lyu S., Yao F., Liang C., Yang X., Guo J., Guo Z. and Gu J., Polyaniline assisted uniform dispersion for magnetic ultrafine barium ferrite nanorods reinforced epoxy metacomposites with tailorable negative permittivity, *Journal of Physical Chemistry C,* **121** (24), 13265–13273 (2017).

7. Wang X., Liu X., Yuan H., Liu H., Liu C., Li T., Yan C., Yan X., Shen C. and Guo Z., Non-covalently functionalized graphene strengthened poly (vinyl alcohol), *Materials and Design Journal,* **139**, 372–379 (2018).

8. Ghasemi M., Naushad M., Ghasemi N. and Khosravi-fard Y., Adsorption of Pb(II) from aqueous solution using new adsorbents prepared from agricultural waste: Adsorption isotherm and kinetic studies. *Journal of Industrial and Engineering Chemistry*, **20**, 2193–2199 (2014).

9. Zhu J., Chen M., Qu H., Wei H., Guo J., Luo Z., Haldolaarachchige N., Young D.P., Wei S. and Guo Z., Positive and negative magnetoresistance phenomena observed in magnetic electrospun polyacrylonitrile-based carbon nanocomposite fibers, *Journal of Materials and Chemistry C*, **2**,

715–722 (2014).

10. Ghaedi M., Hajjati S., Mahmudi Z., Tyagi I., Agarwal S., Maity A. and Gupta V.K., Modeling of competitive ultrasonic assisted removal of the dyes–Methylene blue and Safranin-O using $Fe_3O_4$ nanoparticles, *Chemical Engineering Journal*, **268**, 28–37 (2015).

11. Huang D., Xue W., Zeng G., Wan J., Chen G., Huang C., Zhang C., Cheng M. and Xu P., Immobilization of Cd in river sediments by sodium alginate modified nanoscale zero-valent iron: Impact on enzyme activities and microbial community diversity. *Water Research Journal,* **106**, 15–25 (2016).

12. Huang D., Hu C., Zeng G., Cheng M., Xu P., Gong X., Wang R. and Xue W., Combination of Fenton processes and biotreatment for wastewater treatment and soil remediation. *Sci Total Environment Journal,* **574**, 1599–1610 (2017).

13. Xue W., Huang D., Zeng G., Wan J., Zhang C., Rui X., Cheng M. and Deng R., Nanoscale zero-valent iron coated with rhamnolipid as an effective stabilizer for immobilization of Cd and Pb in river sediments. *Journal of Hazardous Materials,* **341**, 381–389 (2018).

14. Zhang K., Li G.H., Feng L.M., Wang N., Guo J., Sun K., Yu K.X., Zeng J.B., Li T., Guo Z. and Wang M., Ultralow percolation threshold and enhanced electromagnetic interference shielding in poly (L-lactide)/multi-walled carbon nanotube nanocomposites with electrically conductive. *Journal of Materials and Chemistry C,* **5** (36), 9359–9369 (2017).

15. Peng L., Qin P., Lei M., Zeng Q., Song H., Yang J., Shao J., LiaoaB. and Gu J., Modifying $Fe_3O_4$ nanoparticles with humic acid for removal of Rhodamine B in water. *Journal of Hazardous Materials,* **209** (210), 193-198 (2012).

16. P.K. Gautam, S. Banerjee, S.Soni and M.C. Chattopadhyaya, Removal of Ni(II) by magnetic nanoparticles. Journal of Molecular Liquids, 204, 60-69 (2015).

17. Amiri M., Salavati-Niasari M., Pardakhty A., Ahmadi M. and Akbari A., Caffeine: A novel green precursor for synthesis of magnetic $CoFe_2O_4$ nanoparticles and pH-sensitive magnetic alginate beads for drug delivery. *Materials Science and Engineering Journal C*, **76**, 1085-1093 (2017).

18. Guyo U., Makawa T., Moyo M., Nharingo T., Nyamunda B.C. and Mugadza T., Application of response surface methodology for Cd(II) adsorption on maize tassel-magnetite nanohybrid adsorbent. *Journal of Environmental Chemical Engineering,* **3** (Part A), 2472–2483 (2015).

19. Zhang G., Liu Y., Xie Y., Yang X., Hu B., Ouyang S., Liu H. and Wang H., Zinc adsorption on Na-rectorite and effect of static magnetic field on the adsorption. *Applied Clay Science Journal,* **29**, 15-21 (2005).

20. Li N., TianY.,Zhao J., Zhan W., Du J., Kong L., Zhang J. and Zuo W., Ultrafast selective capture of sewage by 3D $Fe_3O_4$@ZnO via weak magnetic field enhanced adsorption. *Chemical Engineering Journal,* **341**, 289-297 (2018).

21. Azzam M.A., El-Wakeel S.T., Mostafa B.B. and El-Shahat M.F., Removal of Pb, Cd, Cu and Ni from aqueous solution using nano scale zero valent iron particles. *Journal of Environmental Chemical Engineering,* **4**, 2196–2206 (2016).

22. Han Y., Wu J., Cheng C., Nagarajan D., Lee C., Li Y., Lo Y. and Chang J., Recovery of gold from industrial wastewater by extracellular proteins obtained from a thermophilic bacterium: Tepidimonasfonticaldi AT-A2. *Bioresource Technology,* **239**, 160-170 (2017).

23. Sheela T. and Nayaka Y.A., Kinetics and thermodynamics of cadmium and lead ions adsorption on NiO nanoparticles. *Chemical Engineering Journal,* **191**, 123-131 (2012).

24. Lagergren S., About the theory of so-called adsorption of soluble substances, *Kungliga Svenska Vetenskapsakademiens. Handlingar*, **24**, 1–39 (1898).

25. Ho Y.S. and Mckay G., A comparison of chemisorption kinetic models applied to pollutant removal on various sorbent, *Trans. I Chem E,* **76** (part B), 332-340 (1998).

26. Liua H., Wanga Z., Lib H.,Wangc H. and Yua R., *Materials Research Bulletin* **100**, 302–307 (2018).

27. Weber W.J. and Morris J.C., Kinetics of adsorption on carbon from solution. *Journal of the Sanitary Engineering Division - American Society of Civil Engineers,* **89**, 31-60 (1963).

28. Xiong T., Yuan X., Chen X., Wu Z., Wang H., Leng L., Wang H., Jiang L. and Zenga G., *Applied Surface Science* **427**, 1107–1117 (2018).

29. Langmuir I., The adsorption of gases on plane surfaces of glass, mica and platinum. *American of Chemical Society Journal,* **57**, 1361-1403 (1918).

30. Tan B., Zhao H., Zhang Y., QuanX., He Z., ZhengW. and Shi B., Amphiphilic PA-induced three-dimensional graphene macrostructure with enhanced removal of heavy metal ions, *Journal*

*of Colloid and Interface Science,* **512**, 853–861 (2018).

31. Freundlich H., Adsorption in solution, *Zeitschrift Physikalische Chemie,* **57**, 384-470 (1906).

32. Temkin M.I. and Pyzhev V., Kinetics of ammonia synthesis on promoted iron catalysts. *Acta Physiochem,* **SSR 12**, 217–222 (1940).

33. Dubinin M.M. and Radushkevich L.V., Equation of the characteristics curve of activated charcoal. Chemisches Zentralblatt, **1**, 875-890 (1947).

34. Şahan T., Erol F. and Yılmaz Ş., Mercury(II) adsorption by a novel adsorbent mercapto-modified bentonite using ICP-OES and use of response surface methodology for optimization. *Microchemical Journal,* **138**, 360–368 (2018).

35. Dickerson, R. E.; Geis, I., *Chemistry, Matter, and the Universe.* USA: W. A. Benjamin Inc. ISBN 0-19-855148-7 (1976).

36. Ives, D. J. G., *Chemical Thermodynamics.* University Chemistry. *Macdonald Technical and Scientific*. ISBN 0-356-03736-3 (1971).

37. Atkins, Peter; Paula De., Julio (10 March 2006). *Physical Chemistry* (8th ed.). W. H. Freeman and Company. p. 212.ISBN 0-7167-8759-8 (2016).

38. Jang J.and Lee D.S., Magnetite nanoparticles supported on organically modified montmorillonite for adsorptive removal of iodide from aqueous solution: Optimization using response surface methodology. *Sci Total Environment Journal*, **615**, 549–557 (2017).

39. Singh B. and Das S.K., Removal of Cu(II) ions from aqueous solution and Industrial effluent using natural aguricultural wastes. *Colloids and Surface.B; Biointerfaces,* **107**, 97– 106 (2013).

40. Wołowicz A. and Hubicki Z., Carbon-based adsorber resin Lewatit AF 5 applicability in metal ion recovery. *Microporous and Mesoporous Materials*, **224**, 400-414 (2016).

41. Naushad M., AL Othman Z.A., Inamuddin and Javadian H., Removal of Pb(II) from aqueous solution using ethylene diamine tetra acetic acid-Zr(IV) iodate composite cation exchanger: Kinetics, isotherms and thermodynamic studies. *Journal of Industrial and Engineering Chemistry,* **25**, 35–41 (2015).

42. Anirudhan T. S. and Radhakrishnan P.G., Thermodynamics and kinetics of adsorption of Cu(II) from aqueous solutions onto a new cation exchanger derived from tamarind fruit shell. *Journal of Chemical Thermodynamic*, **40**, 702–709 (2008).

## تحضير وتوصيف جسيمات اكسيد حديديك مغناطيسية بحجم النانو وتطبيقها في ازالة ايونات الحديد من المحاليل المائيه والمياه الجوفية

**عبـدالسميـــع أحمـد سويـلم[١]، مجدى محمد بهى الدين عواد[١]، يحيى رجب عبد العظيم جدامى[٢]، أحمد توفيق بدير[١]**

[١]قسم الكيمياء - كلية العلوم - جامعة الأزهر - القاهرة - مصر.

[٢]مركز بحوث الصحراء - القاهرة - مصر.

تم تحضير جزيئات أكسيد الحديد النانوية المغناطيسية في المعمل بواسطة طريقة الترسيب وتم معرفة خصائص اكسيد الحديد المغناطيسى بواسطة استخدام التحليل الطيفي بالأشعة تحت الحمراء (FT-IR)، مقياس إنكسار الأشعة السينية (XRD)، المجهر الإلكتروني الماسح (SEM). تم اختبار خصائص إمتزاز جزئيات أكسيد الحديد المغناطيسية لأيونات الحديد بشكل منهجي، بما في ذلك تأثير الأس الهيدروجيني، الجرعة الممتزة، التركيز الأولي، درجة الحرارة، توازن الامتصاص وحركية الامتصاص. تمت دراسة حركية الامتزاز من خلال نماذج pseudo first order و pseudo second order. تم وصف Adsorption isotherm لازالة أيونات الحديد بواسطة نماذج D-R، Freundlich، Langmuir و Temkin isotherm. أظهرت النتائج التي تم الحصول عليها أن أقصى قدرة امتزاز لأيونات الحديد كانت 28.225مجم/جم ونسبة الإزالة وصلت إلى ما يقرب من 85٪ عند الجرعة الممتزة 0.22جم، ودرجة حراره 600درجة مئوية، ووقت مستغرق 210دقيقة، وأس هيدروجينى 4، وتركيز 117.25 مجم/لتر. وجد أن قدرة الامتزاز تزداد مع زيادة درجة الحرارة وانخفاض الجرعة الممتزة. لوحظ أن التفاعل يتفق مع كل من التماذج الأتيه

the pseudo second-order model and Langmuir isotherm mod

أيضا، تم معرفة أن تفاعل امتصاص أيونات الحديد كيميائي. مع معاملات الانحدار عالية للأيونات الحديد، وأثبتت الحسابات الديناميكية الحرارية أن امتزاز أيونات الحديد على جزيئات أكسيد الحديد المغناطيسي هو عملية ماصة للحرارة.